Electrochimica Acta 127 (2014) 228–238

Contents lists available at ScienceDirect

Electrochimica Acta

journal homepage: www.elsevier.com/locate/electacta

Synthesis and Electrochemical Characterization of Ni Nanoparticles by Hydrazine Reduction using Hydroxyethyl cellulose as Capping Agent

E. Ramírez-Meneses[a,*], A.M. Torres-Huerta[b], M.A. Domínguez-Crespo[b], M.G. Ponce-Varela[b], M.A. Hernández-Pérez[c], I. Betancourt[d], E. Palacios-González[e]

[a] Departamento de Ingeniería y Ciencias Químicas, Universidad Iberoamericana, Prolongación Paseo de la Reforma 880, Lomas de Santa Fe. C.P. 01219, México
[b] Centro de Investigación en Ciencia Aplicada y Tecnología Avanzada-Instituto Politécnico Nacional Unidad Altamira, Km 14.5 Carretera Tampico-Puerto Industrial. C.P. 89600 Altamira, Tamaulipas, México
[c] Departamento de Ingeniería en Metalurgia y Materiales. ESIQIE, Instituto Politécnico Nacional, UPALM Zacatenco, D.F., 07738, México
[d] Instituto de Investigaciones en Materiales, Universidad Nacional Autónoma de México, C.P., D.F 04510 México
[e] Laboratorio de Microscopia de Ultra alta Resolución. Instituto Mexicano del Petróleo, Eje Central Lázaro Cárdenas No.152, C.P., 07730, México

ARTICLE INFO

Article history:
Received 5 November 2013
Received in revised form 31 January 2014
Accepted 1 February 2014
Available online 15 February 2014

Keywords:
Chemical synthesis
Nickel nanostructures
Electrode materials
Cyclic voltammetry
Electrochemical impedance spectroscopy.

ABSTRACT

The controlled-size synthesis of well-dispersed metal nanoparticles has been the aim of many research works during the last two decades. In this context, simple and controlled methods are the most suitable to obtain metal nanoparticles. The reduction of transition metal salts in solution is the most widely used method for generating colloidal suspensions of metals. In this work, nickel nanoparticles were synthesized from $NiCl_2{\cdot}6H_2O$ in an ethanol solution with hydrazine hydrate and an appropriate amount of NaOH in the presence of hydroxyethyl cellulose (HEC) used as a capping agent to avoid the coalescence of the nanostructures. Size effects on the nickel nanostructures were studied by varying the concentration of the reducing agent and temperature. The obtained nickel nanostructures were characterized by X-ray diffraction (XRD), showing a face-centered cubic (fcc) structure. Particle sizes from 7 to 13 nm were determined by the Scherrer equation. Scanning electron microscopy (SEM) and transmission electron microscopy (TEM) showed spherical sponge-like nanostructures formed by thin laminar structures. Additionally, infrared spectroscopy showed the presence of HEC functional groups on the surface of the nickel nanostructures after the purification step. Finally, the obtained Ni nanostructures were also characterized by electrochemical techniques and magnetic measurements to determine their electrocatalytic properties and magnetic response, respectively.

1. Introduction

During the past decades, nanomaterials have been of great research interest due to their unique optical, electrical and magnetic properties and their wide range of applications in catalysis, solar cells, light-emitting diodes, biological labeling, electronic fields, etc. It is well known that size, shape and surface state of metallic nanoparticles (NPs) exert great influence on their properties [1]. For this reason, considerable efforts have been done to develop easy and well-defined synthesis methods in order to control the size and shape of metal particles. Parameters such as precursors, nature and percentage of ligand coverage seem to modulate the size and shape of the obtained metal nanoparticles. Ni is one of the transition metals that exhibits magnetism as bulk material and other interesting properties and applications. Ni nanoparticles have a wide variety of applications such as permanent magnets, magnetic fluids, magnetic recording media, fuel cell electrodes, and catalyst [2,3]. Thus, the synthesis of Ni nanoparticles is still an important research area. Numerous approaches such as electrochemical reduction [4], anodic arc plasma [5], organometallic approach [6–8], chemical reduction through microwave-assisted synthesis [9], thermal decomposition [10], polyol [11,12], gas phase reduction [13] and other routes have been developed to obtain Ni nanoparticles. The reported reducing agents include potassium or sodium borohydrides, sodium hypophosphite and hidrazine. Numerous publications have reported the reduction of Ni^{2+} by hydrazine to produce non-agglomerated spherical nickel nanoparticles usually having a rough or spiky surface [14–17]. Bai et al. have

* Corresponding author.
E-mail addresses: esther.ramirez@ibero.mx, esthervincent@yahoo.com (E. Ramírez-Meneses).

http://dx.doi.org/10.1016/j.electacta.2014.02.004
0013-4686/

demonstrated that nickel nanostructures with uniform size and smooth surface could be obtained using water or ethanol as solvent and hydrazine as reducing agent via the solvothermal route with a reaction temperature ranging from 60 to 180 °C [18]. By using water as solvent, the authors observed, through the structural analysis, the presence of metallic Ni powders and $Ni(OH)_2$. On the other hand, the use of ethanol instead of water induces the formation of pure metallic Ni powders. The results also showed that the particles had a spiky surface and their sizes were increased from 50 to 150 nm as the reaction temperature was decreased from 180 to 60 °C. Alternatively, Wu and Chen reported the synthesis of Ni nanoparticles by hydrazine reduction of nickel chloride in ethylene glycol at 60 °C without any protective agent. The authors observed that the mean diameter of the nickel particles (between 6 and 13 nm) was decreased when the $[N_2H_5OH]/[NiCl_2]$ ratio was increased, reaching a constant mean size when $[N_2H_5OH]/[NiCl_2]>12$ [19].

More recently, Mathew et al. obtained flower-like-Ni-nanocone structures in absence of a template or surfactant. The authors showed that the hydrazine reducing power depends on temperature, where nickel ions in solution were reduced after 2 minutes at 60 °C; in this context, a highly alkaline medium (pH ≥ 12) in presence of NaOH is needed for the formation of Ni nanostructures [20]. Thus, at 60 and 90 °C, the authors obtained spherical Ni nanoparticles with a spiky surface and flower-like Ni nanostructures, both of them > 500 nm in size. They concluded that the surface and size of nickel particles are influenced by the initial concentration of Ni^{2+} ions, the synthesis temperature, magnetic stirring and the use of hydrazine hydrate.

Most works have demonstrated that the presence of a stabilizer or capping agent is not necessary to obtain isolated nickel nanoparticles when hydrazine hydrate is employed for the reduction of nickel chloride. As far as we know, only few works have been reported on the synthesis of nickel nanoparticles in the presence of a capping agent by chemical reduction with hidrazine. Some of them are shown in Table 1.

The use of a capping agent plays an important role regarding the surface of the particles by controlling their surface chemistry and growth. In this context, we propose the synthesis of nickel particles from $NiCl_2$ and hydrazine used as a reducing agent by means of a synthetic procedure based on a modified version of methods developed by Mathew, Wang and Chen [14,20,29] in the presence of hydroxyethyl cellulose (HEC) in ethanol. The syntheses were carried out at different temperatures (60-90 °C) and hydrazine concentrations (1-1.4 M). The obtained Ni nanoparticles were also characterized by electrochemical techniques to determine their electrocatalytic properties.

2. Experimental

2.1. Synthesis of metallic nanoparticles

Materials. Hydroxyethyl cellulose (Fluka); $NiCl_2{\cdot}6H_2O$ (≥ 99%, Sigma Aldrich), CH_3CH_2OH (99.5%, Reproquifin,); $N_2H_4{\cdot}6H_2O$ (≥ 99%, Merck); NaOH (98.3%, Fermont) and deionized (DI) water. All chemicals were used without further purification.

The synthesis of Ni nanoparticles was based on the experimental procedure reported previously by A. Mathew et al. [20]. This procedure was modified by using a system without stirring during the synthesis and hydroxyethyl cellulose (HEC) as a capping agent. In the synthesis, HEC, which was the capping agent with a weight ratio of 1:0.04, was added to the green transparent $NiCl_2{\cdot}6H_2O$ (0.1 mmol) ethanol solution (10 mL). Then, hydrazine, $N_2H_4{\cdot}$(1 to 1.4 M, 10 mL) was added dropwise to the solution under vigorous stirring. At this stage, the solution became blue immediately, revealing the formation of the $[Ni(N_2H_4)_3]^{2+}$ complex [30]. After, the solution pH was adjusted at 12 by adding NaOH solution (1 M) and heating at 60-90 °C for 6 h until black powder precipitated completely, indicating the formation of Ni nanoparticles. The formation of Ni NPs was not observed after 6 h at room temperature, when pH was adjusted at 12. Finally, the product was separated by centrifugation, washed with DI water (3 × 20 mL) to remove by-products [15], and dried under vacuum.

2.2. Characterization

X-ray diffraction patterns were recorded with a Bruker Focus X-ray diffractometer using CuKα radiation. The crystallite size was estimated using Scherrer equation, $D = 0.9\lambda/(B\cos\theta)$, where D is the average crystal size, λ is the X-ray wavelength (0.15405 nm for Cu Kα), B is the full width-at-half-maximum height of a diffraction peak at θ angle, which is the angle of the considered Bragg reflection. Fourier transform-infrared spectroscopy (FT-IR, Spectrum One Perkin Elmer) was used to confirm the presence of HEC at the surface of the particles after the purification step. For this analysis, a small quantity of each sample was ground with KBr (Aldrich, 99% IR grade) and the mixture was pressed into a pellet. Thermogravimetric analysis/Differential scanning calorimetry (TGA/DSC) were performed using a SETARAM Instrumentation LABSYS EVO at a temperature range of 30–450 °C with a heating rate of 10 °C/min, using argon flow. Morphological characterization was performed with an Ultra High Resolution Scanning Electron Microscope (UHR-SEM, Dual Beam Nova200 Nanolab microscope) and transmission electron microscopy on a JEOL-1200 EX electron microscope, operating at 120 KV. The magnetic behavior was determined for the samples synthesized at different temperatures (60-90 °C) and 1.4 M hydrazine by means of magnetization M measurements as functions of the applied field H (M-H curves) using a VersaLab Vibrating Sample Magnetometer with a maximum H of 30000 Oe. Finally, in order to determine electrocatalytic properties, Ni nanoparticles were prepared as electrode materials and electrochemical tests were carried out using a Gamry Reference 600™ potentiostat/galvanostat/ZRA.

3. Results and discussion

Z. Li et al. showed that N_2H_4 is able to reduce Ni^{2+}, H^+ and itself under pH from 0 to 14 [15]. The authors suggest that the reduction of Ni^{2+} by N_2H_4 in basic medium occurs in three stages as follows:

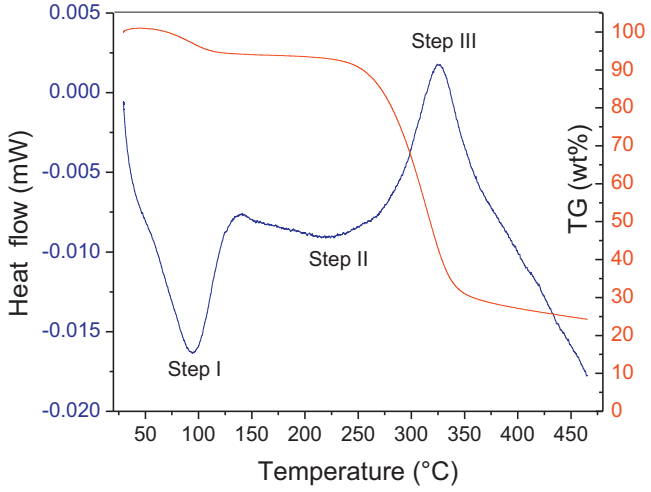

Fig. 1. TGA and DSC curves for HEC.

Table 1
Overview of some different capping agents employed to stabilize nickel nanoparticles using hydrazine as reducing agent.

Ni Precursor	pH value in the raction media	Capping agent or reaction media	Size/shape of nanostructures	Reaction Temperature [°C]	Year of publication	Reference
$NiCl_2$	NaOH pH = not available	Ethylene glycol	~12 nm	90	2012	[21]
$NiCl_2$	NaOH pH = not available	Polyvinyl Pyrrolidone (PVP)	~3 nm	60	2011	[22]
$NiCl_2$	Saturated sodium carbonate solution pH =10.2	sodium dodecyl sulfate and PVP	10-30 nm/spherical particles	40, 60 and 100	2010	[23,24]
$NiCl_2{\cdot}6H_2O$	NaOH pH =11	Hydroxyethyl carboxymethyl cellulose (HECMC)	~31 nm/nearly spherical	80	2008	[25]
$Ni(NO_3)_2{\cdot}6H_2O$	NaOH pH =11	Cetyl-trimethyl ammonium bromide (CTAB)	500-2000 nm/Nanobelt, nanosheet, urchin-like Ni nanocrystals	120-180	2006	[26]
$NiCl_2$	NaOH pH =12	Water/CTAB, *n*-butanol/*n*-octane	6-8 nm and length = 100 nm/needle-like NPs	70	2005	[27]
$NiCl_2$	NaOH pH =10.5	Ethylene glycol	9.2 nm	60	2003	[19]
$NiCl_2$	NaOH/acetone pH =10.6	CTAB/tetra dodecyl ammonium bromide	10-36 nm	60	2002	[28]
$NiCl_2$	Ammonia solution pH =13	Water/CTAB/*n*-hexanol	5.8-14.3 nm/spherical particles	70	2000	[14]

Table 2
Cystallite size from XRD patterns of Ni NPs synthesized (*adjusting pH at 12*) stabilized by hydroxyethyl cellulose (ratio metal precursor: hydroxyethyl cellulose was 1:0.04) at different temperatures (60-90 °C) and different hydrazine concentrations: (a) 1 M, (b) 1.1 M, (c) 1.2 M, (d) 1.3 M and (e) 1.4 M.

Temperature (°C)	Sample	$[N_2H_4{\cdot}H_2O]$	Crystallite size * (111)	(200)
60	Ni-HEC-1	1 M	10.20	8.41
	Ni-HEC-2	1.1 M	10.21	8.41
	Ni-HEC-3	1.2 M	10.22	8.40
	Ni-HEC-4	1.3 M	10.21	8.42
	Ni-HEC-5	1.4 M	10.21	7.00
70	Ni-HEC-6	1 M	13.64	10.57
	Ni-HEC-7	1.1 M	13.62	10.52
	Ni-HEC-8	1.2 M	13.63	10.56
	Ni-HEC-9	1.3 M	13.63	10.56
	Ni-HEC-10	1.4 M	10.24	8.43
80	Ni-HEC-11	1 M	13.62	8.41
	Ni-HEC-12	1.1 M	13.62	8.41
	Ni-HEC-13	1.2 M	10.22	7.00
	Ni-HEC-14	1.3 M	13.64	10.57
	Ni-HEC-15	1.4 M	10.22	8.41
90	Ni-HEC-16	1 M	13.62	8.41
	Ni-HEC-17	1.1 M	13.61	7.00
	Ni-HEC-18	1.2 M	10.22	8.41
	Ni-HEC-19	1.3 M	13.62	10.50
	Ni-HEC-20	1.4 M	13.61	8.41

*Obtained from XRD patterns of Ni Nps synthesized *adjusting pH to 12 (Fig. 2)*

a) Reduction of Ni^{2+} in the presence of N_2H_4

$$2Ni^{2+} + N_2H_4 + 4OH^- \rightarrow 2Ni\downarrow + N_2\uparrow + 4H_2O \quad (1)$$

b) Decomposition of N_2H_4

$$N_2H_4 \rightarrow N_2\uparrow + 2H_2\uparrow \quad (2)$$

c) Disproportionation of hydrazine

$$2N_2H_4 \rightarrow N_2\uparrow + 4NH_3\uparrow \quad (3)$$

However, Hussain and Haque indicate that the reducing ability of hydrazine varies with pH, and in a basic medium, it can be oxidized to N_2 instead of NH_3, which occurs in acid medium. In our case, as described by Libor and Zhang, hydrazine reacts with Ni^{2+} in aqueous media to form the hydrazine complex as follows [31]:

$$Ni^{2+} + 3N_2H_4 \leftrightarrow [Ni(N_2H_4)_3]^{2+} \quad (4)$$

$$2[Ni(N_2H_4)_3]^{2+} + 4OH^- \rightarrow 2Ni\downarrow + N_2 + 4H_2O + 5N_2H_4 \quad (5)$$

In this work, the synthesis was carried out at pH of 12 using NaOH solution and an excess of hydrazine in the presence of HEC. However, when pH was adjusted at 12, after reaction time, some of the obtained solutions showed a small quantity of unreacted complex precursor (blue-purple color) in addition to black precipitate. In contrast, an additional experiment showed that by adjusting the pH at 13, only a black precipitated and colorless solution was obtained after reaction time, indicating that the nickel precursor had totally reacted. Some authors have mentioned that by using ethylene glycol instead of ethanol, NaOH not only plays the role of adjusting the pH solution in the formation of Ni nanoparticles, but also that of a catalyst [19]. This could explain the fact that, in some cases, by varying the hydrazine concentration and adjusting pH at 12, the quantity of NaOH added to the reaction media was

not enough. To assure thermal stability of HEC during the reaction (up to 90 °C), TGA and DSC curves for HEC were examined, Fig. 1. From this figure, it can be noticed that HEC shows one-step thermal decomposition between 245 and 350 °C. The TGA curve showed only a slight weight loss below 110 °C under air. In comparison with the DSC curve, step I, this is due to the loss of water. After this step, the DSC curve showed two exothermic peaks at around 110 and 240 °C. The first exothermic peak, step II, was attributed to the decomposition of the extremities of cellulose ether into CO_2 and H_2 elimination. The second exothermic peak, step III can be attributed to the dehydration of saccharide rings, the breaking of C-O-C bonds in the HEC chain and the formation of anhydride with elimination of the water molecule from the two neighboring carboxylic groups of the grafted chains. This last step was also observed by Wang et al. [32]. The following reactions are suggested for the decomposition of HEC (Eqs. 6.1-6.3). This analysis confirms the thermal stability of HEC under the experimental conditions to obtain stabilized Ni particles.

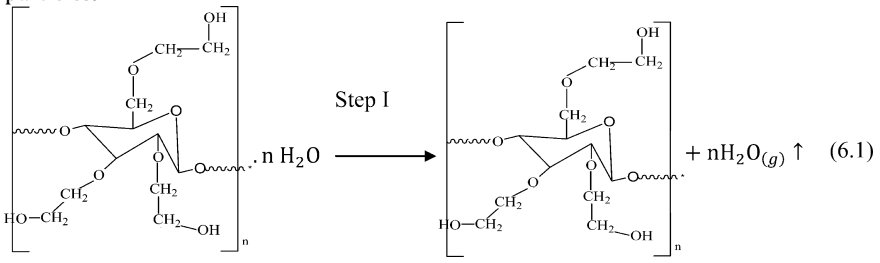

(6.1)

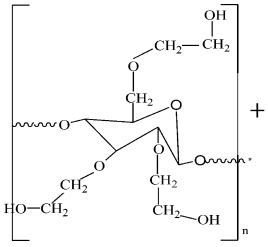

(6.2 a)

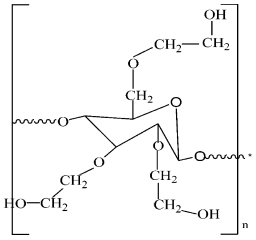

(6.2 b)

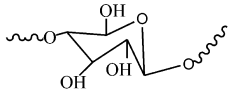

(6.3)

The XRD patterns of the final products are shown in Fig. 2. Samples were obtained using ethanol as solvent, different temperatures (60-90 °C) and hydrazine concentrations (1-1.4 M). It can be seen that all the diffractograms of the samples show (111), (200), (220), (311) and (222) Bragg reflections that are consistent with those of face centered cubic (fcc) Ni (PDF No. 04-0850), indicating the presence of metallic nickel powders. Additionally, the results show that by using ethanol instead of water as solvent, the formation of pure metallic nickel nanoparticles is induced, which is in good agreement with the results reported previously by A. Mathew et al. [20] and L. Bai [18] in absence of capping agents. The formation of Ni nanoparticles is the result of using suitable conditions such as pH and temperature to generate an inert atmosphere, which is formed in this work even by using different hydrazine concentrations (1 to 1.4 M).

The samples prepared in the presence of hydrazine [1 M (80 °C), 1.1 M (60 °C and 90 °C), 1.2 M (60 and 90 °C) and 1.3 M (90 °C)] exhibit an amorphous region between 15 and 35 2θ degrees (Fig. 2). This broad signal corresponds to the holder sample made of amorphous silica. It is important to note that no characteristic peaks of impurities such as nickel oxide or hydroxide were detected. The variation of average crystallite size with the experimental conditions for all the samples of Ni NPs are indicated in Table 2. The values were obtained from the X-ray broadening line obtained from the (111) and (200) peaks using Scherrer equation as previously mentioned.

In general, the changes in crystallite size at different hydrazine concentrations and a fixed reaction temperature are negligible except by using 1.2 and 1.4 M hydrazine; i.e. at these hydrazine concentrations, a reduction in the crystallite size was obtained. These results also indicate that the size of nickel nanoparticles ranges from ~10 to 13 nm (calculated from (111) planes) when the temperature is higher than 60 °C. In almost all the cases, the crystallite size tends to reach a value of ~13 nm when the reaction temperature is ranged from 70 to 90 °C and hydrazine concentration from 1 to 1.4 M.

Alternatively, to determinate the presence of interactions between hydroxyethyl cellulose (HEC) and the surface of the Ni particles, FT-IR analyses were carried out. Fig. 3 shows the FT-IR spectra of the Ni nanostructures stabilized with hydroxyethyl cellulose synthesized in the presence of hidrazine (1-1.4 M) at different reaction temperatures (60-90 °C) and hydroxyethyl cellulose as reference. From the spectrum, it can be seen that this organic stabilizer has vibration peaks corresponding to–OH groups (3200-3400 cm^{-1}), C-O primary alcohols (~1050 cm^{-1}) and C-H stretching

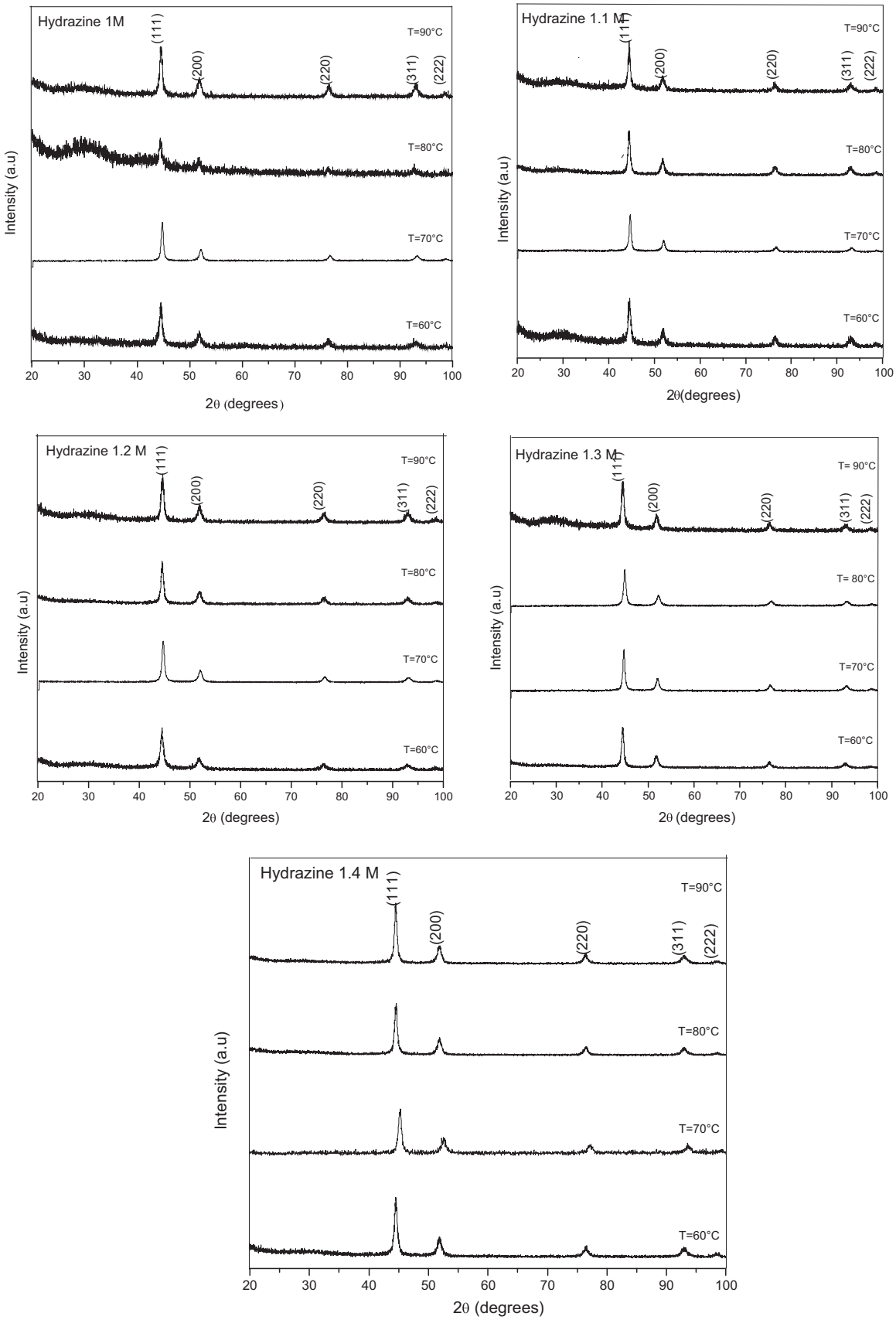

Fig. 2. XRD patterns of Ni NPs synthesized (*adjusting pH at 12*) at different temperatures (60-90 °C) and different hydrazine concentrations: (a) 1 M, (b) 1.1 M, (c) 1.2 M, (d) 1.3 M, and (e) 1.4 M.

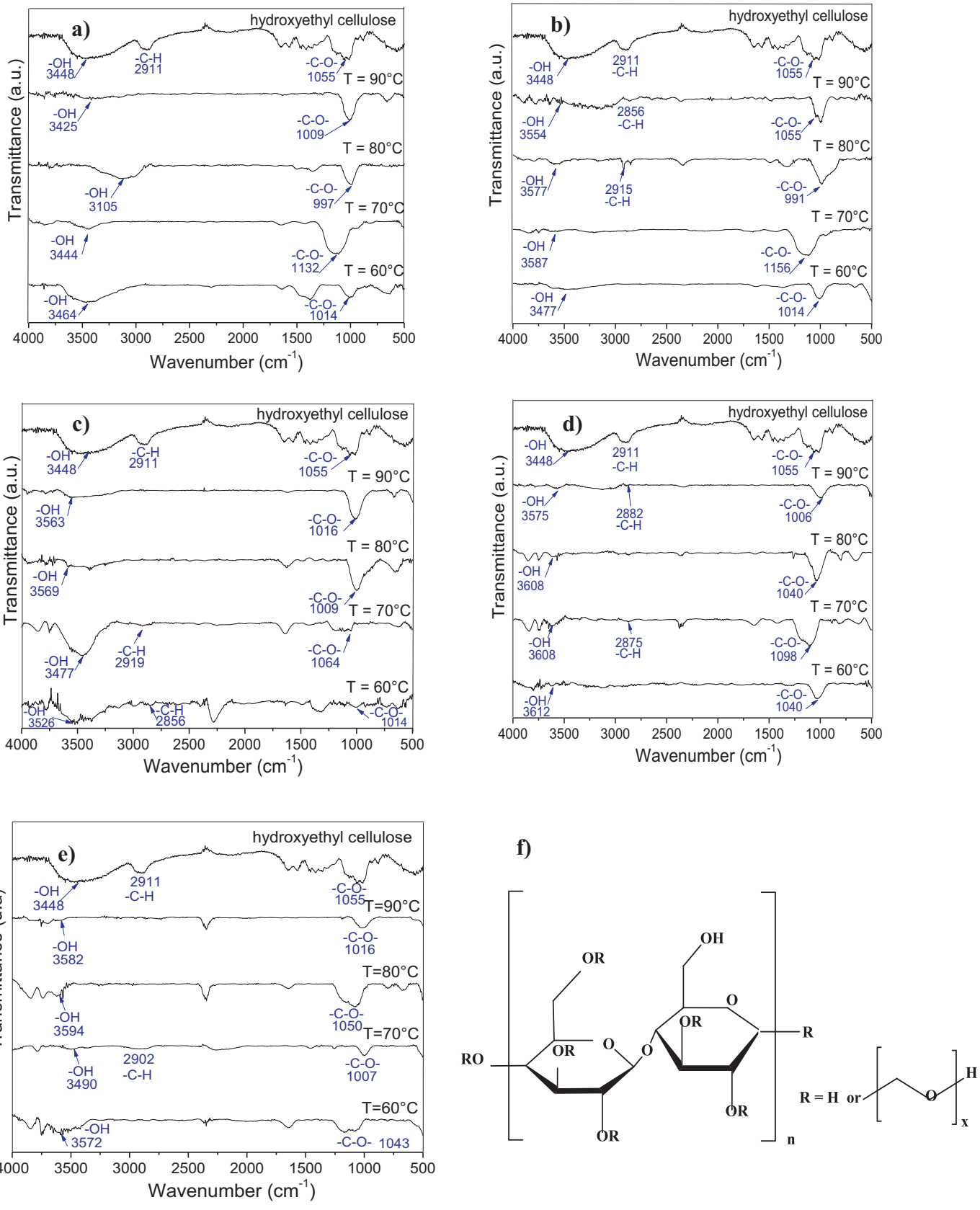

Fig. 3. FT-IR spectra of Ni NPs stabilized with hydroxyethyl cellulose synthesized (*adjusting pH at 12*) at different temperatures in the presence of hydrazine: (a) 1 M, (b) 1.1 M, (c) 1.2 M, (d) 1.3 M and (f) 1.4 M. Additionally, (f) hydroxyethyl cellulose as reference and its corresponding formula.

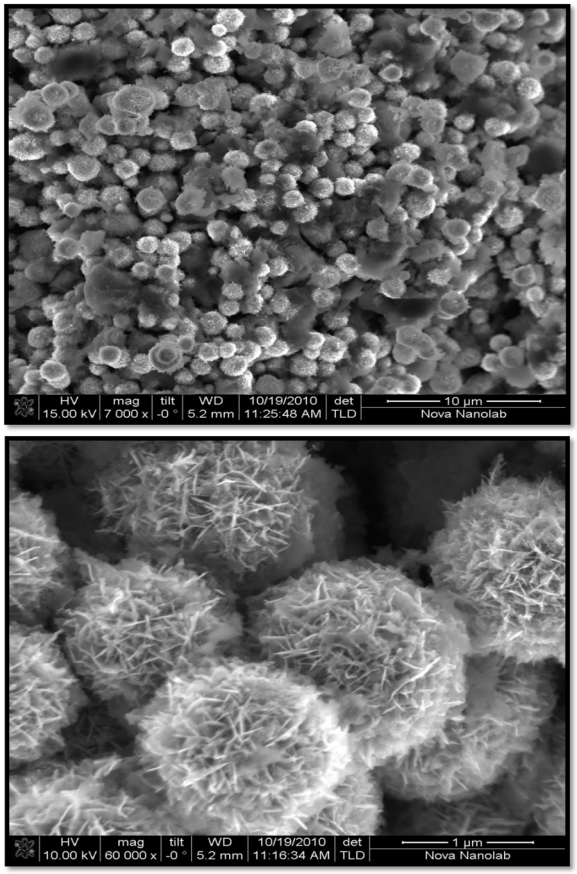

Fig. 4. UHR-SEM micrographs of Ni nanoparticles obtained at 60 °C and 1 M hydrazine.

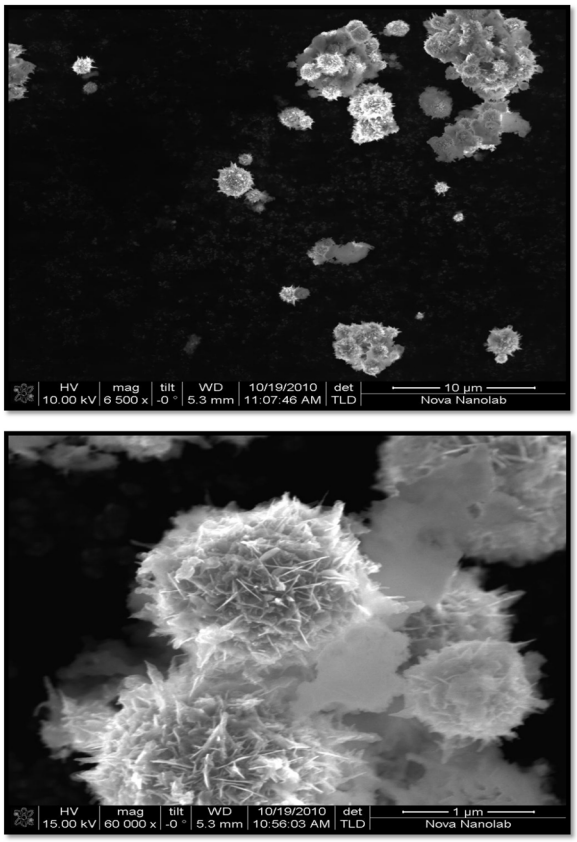

Fig. 5. UHR-SEM micrographs of Ni nanoparticles obtained at 60 °C and 1.4 M hydrazine.

vibrations (~2900 cm^{-1}). The position and relative intensity of these bands from stabilized Ni nanostructures change with respect to the pure hydroxyethyl cellulose. The variation of the C-O and–OH infrared bands suggests the formation of links between the stabilizer and the surface of the nickel nanoparticles.

To confirm the crystallite size of the nickel particles SEM and TEM analyses of selected samples were carried out. Representative SEM micrographs of Ni particles obtained at 60 °C in the presence of 1 and 1.4 M hydrazine are shown in Figs. 4 and 5. As it can be seen, the particles are spherical, sponge-like, and appear to be formed by thin laminar structures; these Ni particles commonly called secondary particles are composed by primary ones (thin laminar structures). These structures could be attributable to the flower-like-structure growth mechanism reported by A. Mathew et al., and S. Nath et al. [20,33]. In this case, it is also suggested that the particles with larger sizes grow at the expense of smaller ones via the Ostwald ripening process, where small particles are dissolved and grow into larger crystals [33].

The sponge-like architecture was further characterized by TEM equipped with selective area electron diffraction (SAED). Fig. 6(a) represents the typical TEM image of as-synthesized sponge-like nickel structures. From the SAED pattern, the presence of Ni atomic planes (Fig. 6b) is confirmed. Thus, the value of the crystallite size determined by the Sherrer equation (7-13 nm) seems to be consistent with the size observed from the TEM image (Fig. 6a) of the thin laminar structures also called primary particles that are organized to form semi-spherical secondary particles. These Ni structures, having the morphologies shown in Figs. 3 and 4, are expected to display better electrocatalytic properties than the metallic Ni.

Table 3
Anodic and cathodic peaks of Ni nanoparticles at different reducing agent concentrations.

Hydrazine concentration (M)	Anodic Peaks E (mV)	Cathodic Peaks E (mV)
1	358	199
		−457
1.1	347	122
		−408
1.2	−461	138
	312	−408
1.3	−196	203
		−438
1.4	304	194
		−444

Then, the Ni particles were prepared as electrode materials to determine their electrocatalytic performance. A vitreous carbon bar (3 mm in diameter) was used as Ni particle support, and a three-way electrochemical cell was employed to carry out the electrocatalytic tests. A saturated Calomel electrode and a graphite bar were used as reference and counter electrodes, respectively. Cyclic voltammetry was performed at room temperature, 20 mVs^{-1} of sweep rate, from -1200 to 500 mV, and HEC as stabilizing agent. Fig. 7 shows the results after 10 potential cycles of Ni nanoparticles synthesized as described above. The presence of one anodic (A) and two cathodic (B) peaks corresponding to the oxidation and reduction of Ni species, respectively, can be seen, except in Fig. 7c, where two anodic (-461 and 312 mV) and two cathodic (138 and -408 mV) peaks are recorded. Burke [34] and Hahn [35] have reported two steps for Ni oxidation process (Eq. 7a-b):

First anodic peak, $Ni^0 + 2OH^- \rightarrow Ni(OH)_2 + 2e^-$ (7a)

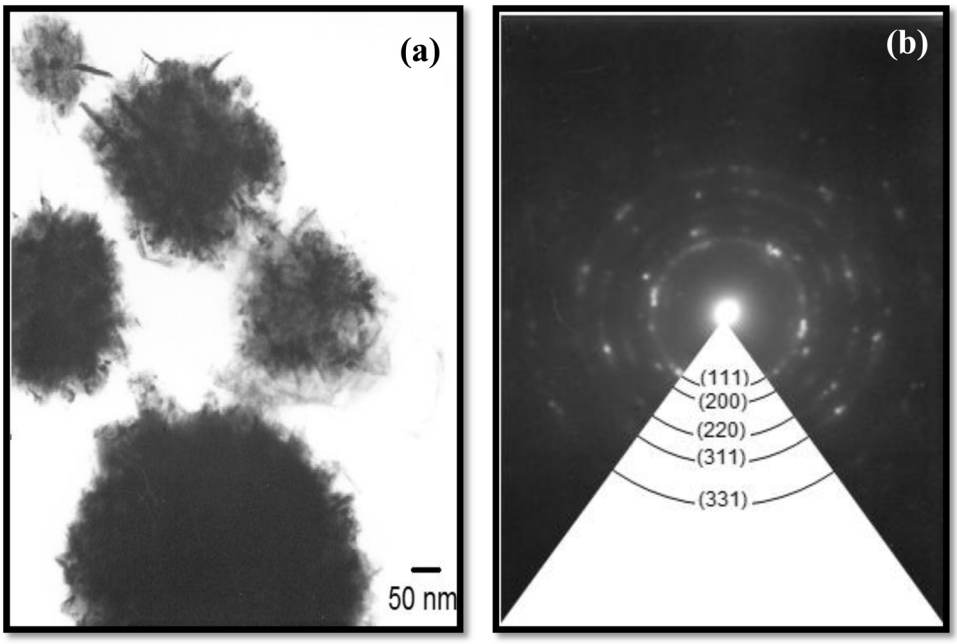

Fig. 6. TEM image of nickel structures obtained at 60 °C and 1.4 M hydrazine (a), and the corresponding SAED pattern (b).

Table 4
EIS parameters of Ni electrodes at different overpotentials, 6 M NaOH using Levenberg- Marquardt method.

Hydrazine concentrations									
Parameters	1 M Overpotential (mV)			1.1 M Overpotential (mV)			1.2 M Overpotential (mV)		
	η = -100	η = -200	η = -300	η = -100	η = -200	η = -300	η = -100	η = -200	η = -300
R_S (ohms*cm^2)	2.37	2.45	1.93	2.05	1.89	2.32	0.70	0.72	0.73
CPE_1 (S*sn)	4.115E-6	1.362E-6	126.6E-6	499.9E-6	637.8E-6	549.6E-6	2.946E-3	2.470E-3	2.170E-3
n_1	0.9932	0.9983	0.6838	0.7	0.5696	0.5608	0.6	0.6921	0.6834
R_{Nps}(ohms*cm^2)	0.0230	0.0473	0.0529	0.1588	0.18	0.3093	0.0509	0.0720	0.0613
CPE_2 (S*sn)	2.032E-3	1.380E-3	667.3E-6	3.081E-3	3.582E-3	3.898E-3	2.440E-3	1.932E-3	1.922E-3
n_2	0.5998	0.6246	0.7622	0.8092	0.7482	0.8078	0.7841	0.8428	0.8287
R_{Tc}(ohms*cm^2)	23.09	1.83	1.10	10.21	13.14	8.8	7.96	1.08	0.91
x^2	26.51E-6	73.16E-6	77.56E-6	137.8E-6	302.5E-6	359.1E-6	167.1E-6	67.67E-6	194.3E-6

Parameters	Hydrazine					
	1.3 M Overpotential (mV)			1.4 M Overpotential (mV)		
	η = -100	η = -200	η = -300	η = -100	η = -200	η = -300
R_S (ohms*cm^2)	1.75	1.81	1.94	2.65	2.11	1.82
CPE_1 (S*sn)	13.81E-6	2.387E-6	10.68E-6	920.4E-6	625.1E-6	77.67E-6
n_1	0.8128	0.9317	0.7681	0.6	0.5907	0.7
R_{Nps}(ohms*cm^2)	0.0576	0.0643	0.1290	0.02	0.0354	0.012
CPE_2 (S*sn)	1.893E-3	1.882E-3	1.857E-3	1.887E-3	1.358E-3	1.079E-3
n_2	0.7056	0.6991	0.6911	0.5884	0.6374	0.675
R_{Tc}(ohms*cm^2)	15.94	16.55	17.64	21.99	2.81	1.98
x^2	183.9E-6	190.6E-6	328.2E-6	38.45E-6	60.31E-6	35.92E-6

Second anodic peak, $Ni(OH)_2 \rightarrow NiOOH + H^+ + e^-$ (7b)

The two cathodic peaks correspond to the reduction process of the formed compounds during the oxidation process. In Fig. 7d, an anodic peak (C) is recorded at -196 mV; this peak is the response of the HEC (Fig. 8). The second cathodic peak is overlapped with that corresponding to Ni.

The hydrogen evolution reaction (HER) is recorded at -1100 mV, according to the following reaction:

$$2H_2O + 2e^- \rightarrow H_2 + 2OH^- \quad (8)$$

Table 3 lists the potentials of anodic and cathodic peaks obtained from Fig. 7. The mismatch among the results of this work and those reported in the literature [8] could be attributed to the stabilizing agent and the reducing agent concentrations used in this work, which can modify the voltammograms and the quantity of adsorbed hydrogen.

The electrochemical impedance spectroscopy (EIS) was performed from 1×10^5 to 1×10^{-1} Hz (ten points of frequency per decade), 10 mV in amplitude and room temperature. Fig. 9 displays the Nyquist plots for the Ni nanoparticles at different

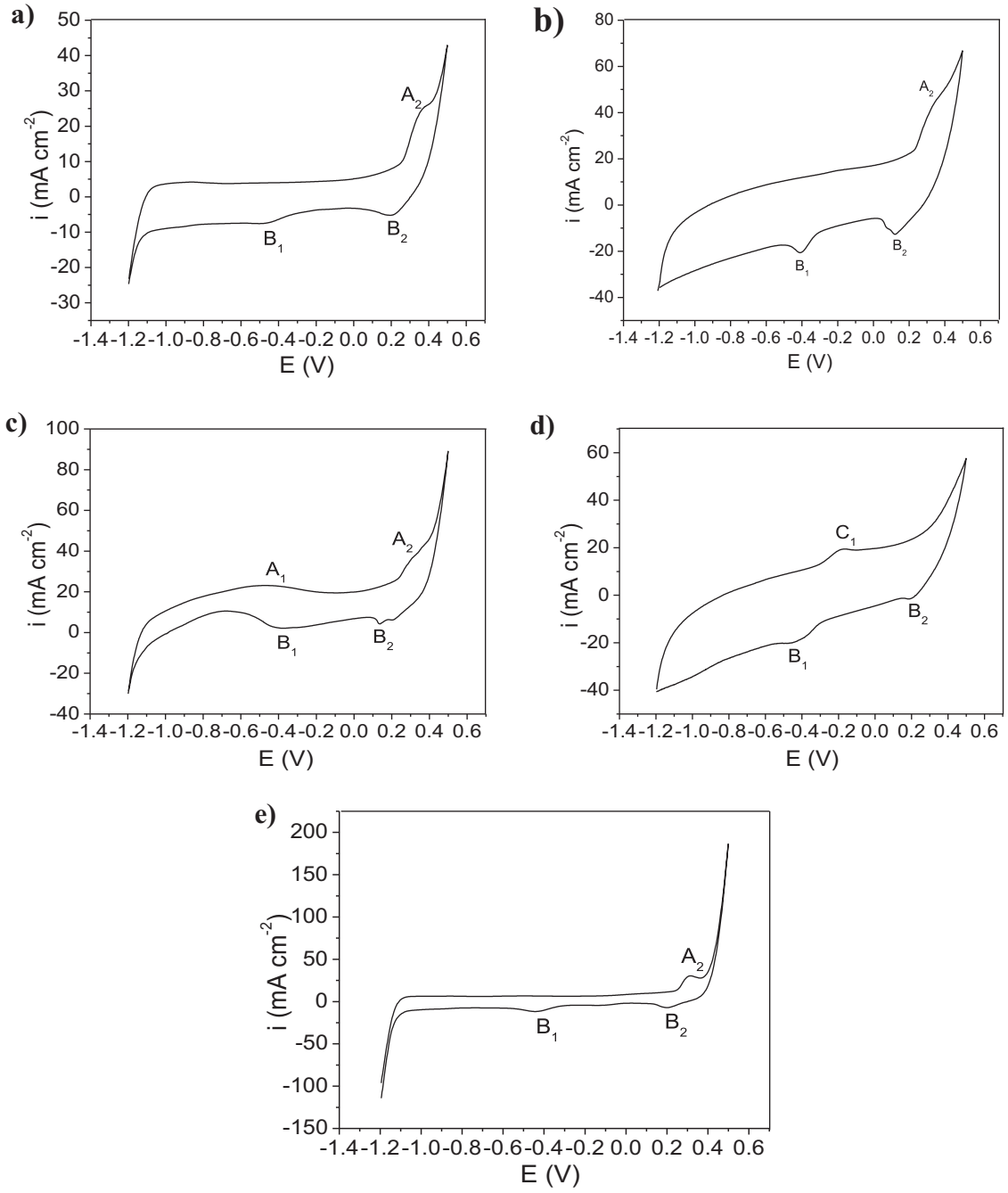

Fig. 7. Cyclic voltammetry plots of HEC stabilized Ni nanoparticles at room temperatura, 6 M NaOH and hydrazine concentrations of: (a) 1 M (b) 1.1 M (c) 1.2 M (d) 1.3 M, and (e) 1.4 M.

overpotentials (η = -100, -200 and -300 mV) and in the HER area. Two semicircles are detected and attributed to the stabilized Ni nanoparticles; 1.2 M hydrazine samples show the lowest electron transfer resistance. The equivalent electric circuit used to explain the EIS results is shown in Fig. 10, and the Levenberg- Marquardt method was employed to simulate the Ni electrode response; the simulation results are reported in Table 4. From the overall results, it is determined that the synthesized Ni nanostructures using a 1.2 M hydrazine concentration presented the lowest charge transfer resistance. The results corroborate that an enhanced of the electro-activity of the electrode materials on HER can be achieved when hydrazine is employed for the reduction of nickel chloride.

It is known that the magnetic properties of nanomaterials are closely related to the size, morphology, crystallinity and composition [36]. The magnetic response of the sponge-like structures for samples synthesized at different temperatures (60-90 °C) and 1.4 M hydrazine is shown in Fig. 11 as *M-H* curves recorded at 298 K for which a typical ferromagnetic response is observed, characterized by hysteresis loops showing saturation magnetization values within the range 60- 48 emu/g range and noticeable coercive fields between 100 - 155 Oe. This ferromagnetic

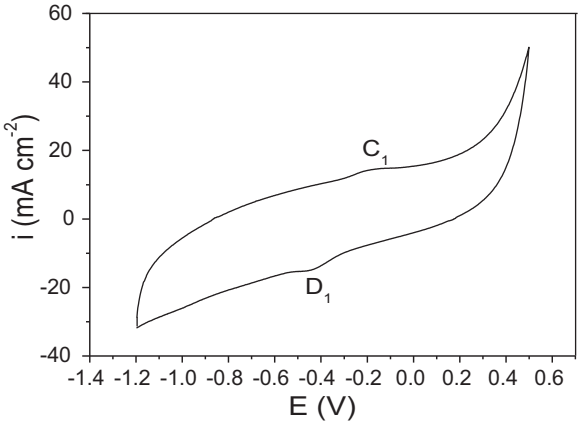

Fig. 8. Cyclic voltammetry of HEC at the same conditions used for Ni nanoparticles.

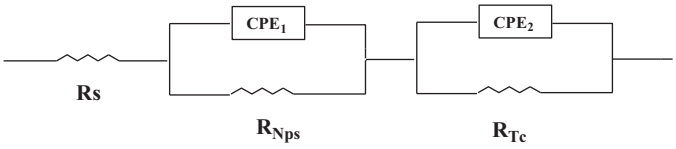

Fig. 10. Equivalent electric circuit proposed for the Ni nanoparticle system.

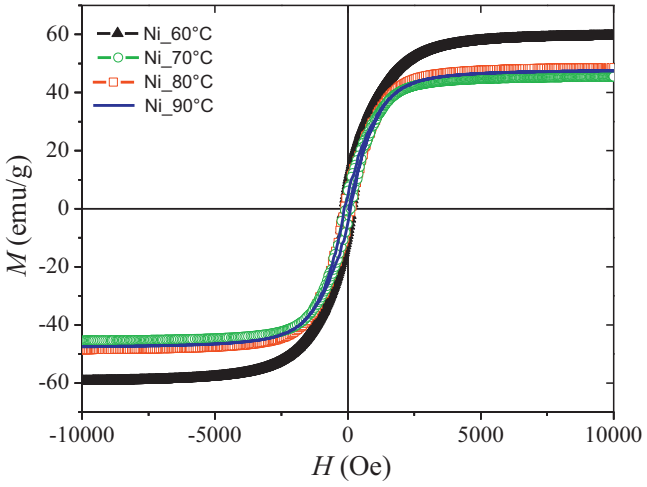

Fig. 11. *M-H* hysteresis loops for the samples synthesized at different temperatures (60-90 °C) and 1.4 M hydrazine concentration showing a typical ferromagnetic behavior.

behavior results from the cooperative interactions of the laminar nanostructures, namely, exchange coupling between magnetic moments afforded by the direct contact of the nanosized entities. This collective behavior precludes the superparamagnetic response associated with Ni nanostructures with mean sizes below 10 nm [37].

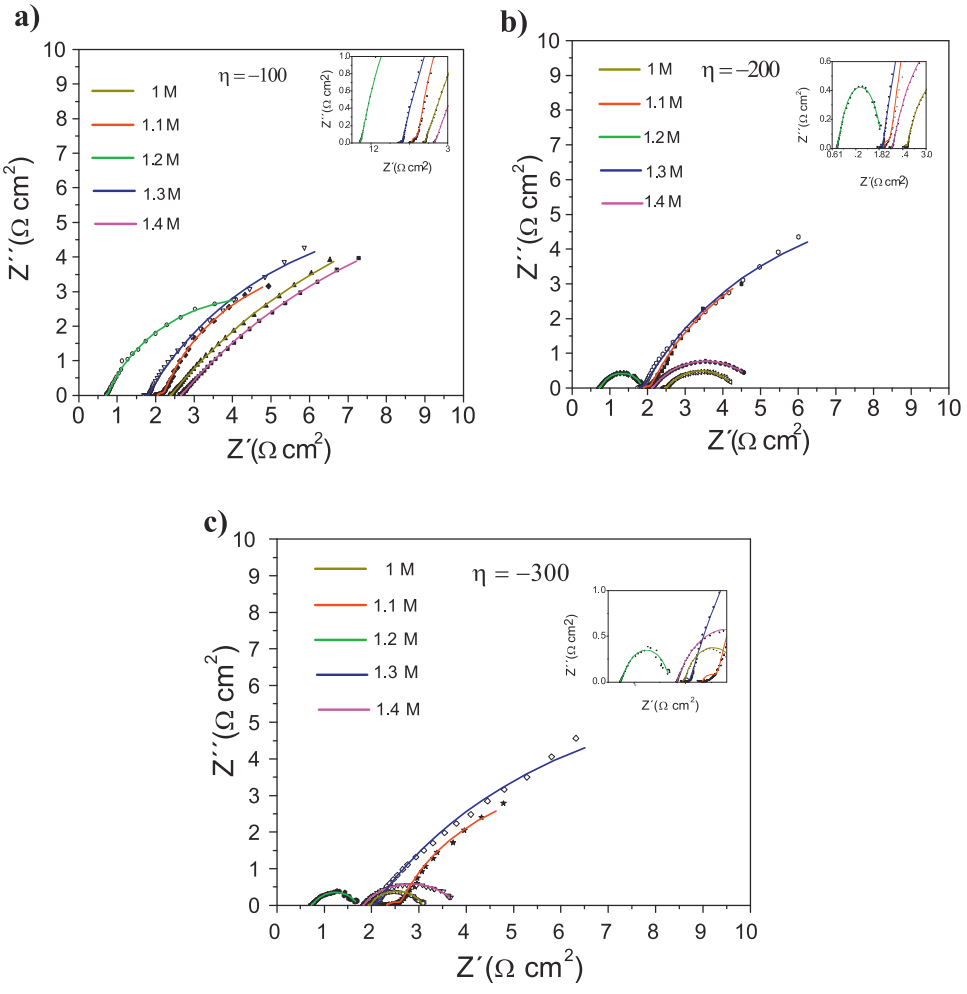

Fig. 9. Nyquist plots of Ni nanoparticles at different hydrazine concentrations in 6 M NaOH, room temperature and a) -100 mV, b) -200 mV, and c) -300 mV.

4. Conclusions

Nickel nanoparticles were synthesized from $NiCl_2$ and hydrazine, stabilized with HEC and characterized by TGA/DSC, FTIR, XRD, SEM, TEM, CV and EIS. From the TGA/DSC, the thermal stability of HEC and its use as Ni-nanoparticle stabilizer was determined. The FT-IR results suggest that HEC interacts with the Ni surface through–C-O-C- and -OH functional groups. According to XRD, Ni is present only as a metal, i. e., another species were not detected at the limit of X-ray diffraction analysis; the crystallite size varied from 7 to 13 nm. Apparently, the hydrazine concentration and HEC favor the formation of thin laminar structures with spherical, sponge-like morphology. All the nanostructures manifested a typical ferromagnetic behavior as a consequence of the exchange interaction among the nanosized laminar structures, which hinders the expected superparamagnetic response of Ni nanoparticles with mean size below 10 nm. Samples synthesized with 1.2 M hydrazine showed the best electrocatalytic performance.

Acknowledgements

The authors wish to acknowledge the financial support provided by: CONACyT through the 157613, 132660 and 133618 projects, and SNI; Dirección de Investigación, Universidad Iberoamericana through the 0053 project; Instituto Politécnico Nacional through the SIP 2014-0164, 2014-0992 and 2013-0404 projects.

References

[1] C. Burda, X. Chen, R. Narayanan, M.A. El-Sayed, Chem. Rev 105 (2005) 1025–1102.
[2] E. Verreli, D. Tsoukalas, K. Giannakopoulos, D. Kouvatsos, P. Normand, D.E. Ioannou, Microelectronic Engineering 84 (2007) 1994–1997.
[3] A. Dhakshinamoorthy, K. Pitchumani, Tetrahedron Lett 49 (2008) 1818–1823.
[4] Q. Cheng, C. Wu, J. Chen, Y. Zhou, K. Wu, J. Phys. Chem. C. 115 (2011) 22845–22850.
[5] Z. Wei, T. Xia, L. Bai, J. Wang, Z. Wu, P. Yan, Mater. Lett 60 (2006) 766–770.
[6] N. Cordente, M. Respaud, F. Senocq, M.J. Casanove, C. Amiens, B. Chaudret, Nano Lett 1 (2001) 565–568.
[7] S. Carenco, C. Boissière, L. Nicole, C. Sanchez, P. Le Floch, N. Mézailles, Chem. Mater 22 (2010) 1340–1349.
[8] M.A. Domínguez-Crespo, E. Ramírez-Meneses, V. Montiel-Palma, A.M. Torres Huerta, H. Dorantes Rosales, Int. J. Hydrogen 34 (2009) 1664–1676.
[9] W. Xu, K.Y. Liew, H. Liu, T. Huang, C. Sun, Y. Zhao, Mater. Lett 62 (2008) 2571–2573.
[10] F. Davar, Z. Fereshteh, M. Salavati-Niasari, J. Alloys Compd 476 (2009) 797–801.
[11] V. Tzitzios, G. Basina, M. Gjoka, V. Alexandrakis, V. Georgakilas, D. Niarchos, N. Boukos, D. Petridis, Nanotechnology 17 (2006) 3750–3755.
[12] G.G. Couto, J.J. Klein, W.H. Schreiner, D.H. Mosca, A.J.A. de Oliveira, A.J.G. Zarbin, J. Coll. Interface Science 311 (2007) 461–468.
[13] Y.J. Suh, H.D. Jang, H.K. Chang, D.W. Hwang, H.C. Kim, Mater. Research Bull 40 (2005) 2100–2109.
[14] D.-H. Chen, S.-H. Wu, Chem. Mater 12 (2000) 1354–1360.
[15] D.-H. Chen, C.-H. Hsieh, J. Mater. Chem 12 (2002) 2412–2415.
[16] Z. Li, C. Han, J. Shen, J. Mater. Science 41 (2006) 3473–3480.
[17] Z.G. Wu, M. Munoz, O. Montero, Advanced Powder Technology 21 (2010) 165–168.
[18] L. Bai, F. Yuan, Q. Tang, Mater. Lett 62 (2008) 2267–2270.
[19] S.-H. Wu, D.-H. Chen, J. Colloid and Interface Science 259 (2003) 282–286.
[20] A. Mathew, N. Munichandraiah, G. Mohan, Rao. Mater, Science and Engineering B. 158 (2009) 7–12.
[21] M. Hemalatha, N. Suryanarayanan, J. Ovonic Research 8 (2012) 47–51.
[22] M. Singh, M. Kumar, F. Štěpánek, P. Ulbrich, P. Svoboda, E. Santava, M.L. Singla, Adv. Mat. Lett 2 (2011) 409–414.
[23] M.S. Hussain, K.M.A. Haque, J. Sci. Res 2 (2010) 313–321.
[24] M.S. Hussain, K.M.A. Haque, A.R. Ghihab, Int. J. Nanoparticles 4 (2011) 33–44.
[25] H. Wang, X. Kou, J. Zhang, J. Li, Bull. Mater. Sci 31 (2008) 97–100.
[26] X. Liu, X. Liang, N. Zhang, G. Qiu, R. Yi, Mater Science Engineering B. 132 (2006) 272–277.
[27] D.E. Zhang, X.M. Ni, H.G. Zheng, Y. Li, X.J. Zhang, Z.P. Yang, Mater. Lett 59 (2005) 2011–2014.
[28] D.-H. Chen, C.-H. Hsieh, J. Mater. Chem 12 (2002) 2412–2415.
[29] H. Wang, X. Kou, L. Zhang, J. Li, Mater Research Bulletin 43 (2008) 3529–3536.
[30] R. Wojcieszak, S. Monteverdi, J. Ghanbaja, M.M. Bettahar, J. Colloids Interf. Sci 317 (2008) 166–174.
[31] Z. Libor, Q. Zhang, Mater. Chem. Physics 114 (2009) 902–907.
[32] W. Wang, J. Wang, Y. Kang, A. Wang, Composites: Part B 42 (2011) 809–818.
[33] S. Nath, S. Jana, M. Pradhan, T. Pal, J. Colloid Interface Sci 341 (2010) 333–352.
[34] L.D. Burke, T.A.M. Twomey, J. Electroanal. Chem 167 (1984) 285–290.
[35] F. Hahn, B. Beden, M.J. Croissant, C. Lamy, Electrochim. Acta 31 (1986) 335–342.
[36] X. Ni, Q. Zhao, D. Zhang, X. Zhang, H. Zheng, J. Phys. Chem. C 111 (2007) 601–605.
[37] E. Ramírez-Meneses, I. Betancourt, F. Morales, V. Montiel-Palma, C.C. Villanueva-Alvarado, M.E. Hernández-Rojas, J. Nanoparticle Research 13 (2011) 365–374.